Nuclear Physics A427 (1984) 526–544

MEASUREMENT OF THE ABSOLUTE CROSS SECTION OF THE ^{3}He(^{4}He, γ)^{7}Be REACTION AT $E_{c.m.} = 525$ keV

T.K. ALEXANDER, G.C. BALL, W.N. LENNARD and H. GEISSEL*

Atomic Energy of Canada Limited Research Company, Chalk River Nuclear Laboratories, Chalk River, Ontario, Canada K0J 1J0

and

H.-B. MAK

Department of Physics, Queen's University, Kingston, Ontario, Canada K7L 3N6

Received 16 April 1984

Abstract: The cross section for the radiative capture reaction ^{3}He(^{4}He, γ)^{7}Be has been measured at 525 keV in the centre-of-mass by detection of prompt capture γ-rays. The targets were ^{3}He-implanted Nb foils that allowed us to circumvent the experimental difficulties inherent in the use of extended gas cells for absolute measurements. The results give an inferred zero-energy cross-section factor of $S_{34}(0) = 0.47 \pm 0.04$ keV · b. The present result is compared with results from previous capture γ-ray yield and ^{7}Be-activity methods of measuring the cross-section factor.

E NUCLEAR REACTIONS ^{3}He(^{4}He, γ), $E = 525$ keV; measured $\sigma(E_{c.m})$, $E_{c.m}$, branching ratio. ^{3}He-implanted Nb target.

1. Introduction

The ^{3}He(^{4}He, γ)^{7}Be reaction rate at low energies affects the predicted solar neutrino flux and bears strongly on the solar neutrino problem [1]. The crucial member of the chain of reactions that leads to the predicted solar neutrino flux measured by the Brookhaven ^{37}Cl solar neutrino detector [2] is the weak (0.02%) branch, ^{3}He(^{4}He, γ)^{7}Be(p, γ)^{8}B$\rightarrow{}^8$Be$+$e$^+ + \nu_e$. (The ^{37}Cl$+\nu_e\rightarrow{}^{37}$Ar$+$e$^-$ reaction is most sensitive to the energetic neutrinos from ^{8}B.) The measured [2] solar neutrino flux is 1.8 ± 0.3 SNU (1 SNU $= 10^{-36}$ captures per ^{37}Cl atom per second), whereas the predicted value is 7.6 ± 3.3 SNU (3σ error) [1].

The ^{3}He(^{4}He, γ)^{7}Be reaction cross section is very difficult to measure at solar energies ($\sim$15 keV); however, measurements in the 100 keV to 1 MeV region have been made, converted to the low-energy S-factor, $S_{34}(E_{c.m.})$, and extrapolated to solar energies with theoretical predictions [3]. The S-factor is related to the cross section $\sigma(E_{c.m.})$ by $S(E_{c.m.}) = \sigma(E_{c.m.})E_{c.m.} \exp(2\pi\kappa)$, where $E_{c.m.}$ is the bombarding energy in the c.m. system and κ is the Sommerfeld parameter. Reported values [4–9])

* On leave from GSI, D-61 Darmstadt, Federal Republic of Germany.

for the zero-energy intercept $S_{34}(0)$ differ by approximately a factor of two. Since $S_{34}(0)$ is an important parameter in the calculation of the solar neutrino flux, the predicted flux is strongly influenced by the adopted value of $S_{34}(0)$ since it varies [1]) approximately as $S_{34}(0)^{0.8}$.

All previous experiments [4–9]) have used gaseous targets of ^{3}He or ^{4}He, bombarded by ^{4}He or ^{3}He beams, respectively. The experiments have employed γ-ray detectors either to observe directly the prompt capture γ-radiation or to detect off-line the delayed ^{7}Be radioactivity induced by bombardment. The most recent experiments [6–9]) have employed high-resolution Ge(Li) or intrinsic Ge spectrometers.

The present experiment is novel in that targets of ^{3}He implanted in Nb foils are used rather than gaseous targets. By this technique, favourable geometry and beam-current integration can be obtained for the absolute determination of the direct-capture γ-ray yield. The areal density and depth distribution of the ^{3}He implanted targets can be accurately determined in auxiliary experiments before and after the γ-ray yield measurements. The ^{3}He concentration in the targets is localized to $\sim$0.1 μm in depth below the surface of the Nb and the inherent experimental difficulties of extended gas cells for absolute measurements are thus circumvented.

2. Experimental apparatus

In the present work, ^{3}He-implanted metallic foils of Nb were used for targets in the specially designed, water-cooled Faraday-cup target assembly shown in fig. 1. During bombardment with 1.3 MeV $^4He^+$ ions of approximately 2.5 μA intensity from the CRNL 2 MV Pelletron accelerator, the capture γ-rays were detected at 0° with a 80 cm^3 Ge(Li) detector located inside a lead shield. The entrance beam line and target regions were shrouded by gold-plated copper, cooled to liquid nitrogen temperature to prevent carbon build-up on the targets during bombardment. We lowered the beam current density at the target by producing a diffuse horizontal line focus and sweeping the position vertically with electrostatic steerers located after the analyzing magnet. The beam was collimated by the two 6 mm diameter Ta apertures shown in fig. 1. A 9 mm aperture grounded to the water-cooled surface protected an electrically insulated 8 mm diameter aperture in front of the Faraday-cup target assembly. During bombardment, the current on this aperture was minimized and was a negligible fraction of the beam on target. A 9 mm diameter electrode in front of the Faraday cup was held at -90 V to repel electrons back to the Faraday cup, which consisted of a copper block with a Ta-lined 10 mm diameter cylindrical hole in it. The block was cooled through a BeO wafer attached to a water-cooled copper surface. The ^{3}He-implanted Nb foil (125 μm thick) backed by a 250 μm thick Au foil covered the end of the cylindrical hole to complete the Faraday cup and the cup-target assembly was connected to a current integrator. This design allowed the target-to-detector distance to be close (approx. 16 mm) and reproducible to obtain good counting sensitivity. To measure the absolute efficiency of the Ge(Li)

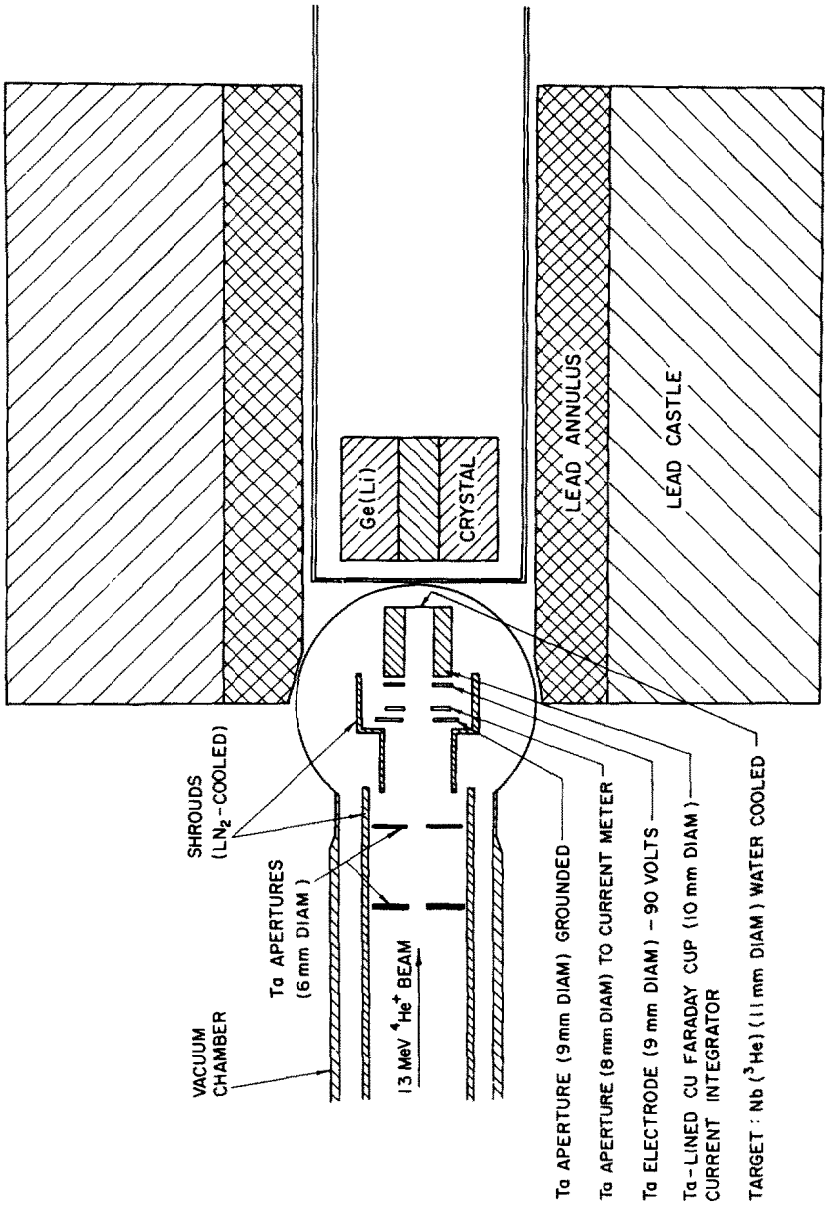

Fig. 1. The target chamber and Ge(Li) detector arrangement for observation of γ-rays from the $^{3}He(^{4}He, \gamma)^{7}Be$ reaction.

detector, weak sources of ^{137}Cs(1.31 kBq ≡ 0.0353 μCi) and ^{88}Y(0.82 kBq ≡ 0.0222 μCi) deposited onto 250 μm thick Au target blanks were prepared by CRNL's standardization group and positioned in the exact target location.

To check the apparatus and the calibration procedures, the thick-target yield of γ-rays per incident proton from the 992 keV resonance of the $^{27}Al(p, \gamma)^{28}Si$ reaction was measured. The yield curve of the 1779 keV γ-rays from the first excited level of ^{28}Si is shown in fig. 2. The target consisted of a 40 μg/cm^2 layer of Al evaporated onto 250 μm thick Ta. The yield of γ-rays measured on the flat part of the resonance curve is related to the strength S_{lab} of the resonance by [10])

$$S_{lab} = (2J_p + 1)(2J_T + 1)\frac{2\varepsilon y}{\lambda^2_{c.m.}},$$

where J_p and J_T are the spin of the proton and target nucleus respectively, ε is the stopping power in units of eV · cm^2/atom, $\lambda^2_{c.m.}$ is the c.m. de Broglie wavelength of the projectile, and y is the yield of γ-rays per incident proton. The predicted yield of 1779 keV γ-rays is $(1.03 \pm 0.06) \times 10^{-9}$ γ/proton based on the branching ratio (94.8 ± 1.5)% given by Anttila *et al.* [11]) and the strength $S_{lab} = 22.9 \pm 1.3$ eV measured by Paine and Sargood [10]). The measured yield was $(0.96 \pm 0.06) \times 10^{-9}$ γ/proton after correction for the 0° yield using the angular distribution Legendre

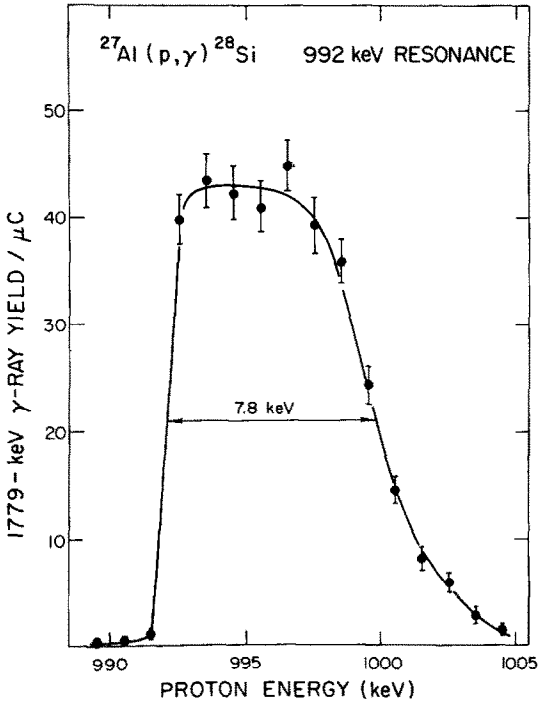

Fig. 2. The yield curve for the 1779 keV γ-ray from the 992 keV resonance of $^{27}Al(p, \gamma)^{28}Si$.

polynomial coefficients given by Anttila *et al.* [11]) ($A_2 = 0.000 \pm 0.003$ and $A_4 = -0.016 \pm 0.003$). Appropriate corrections were also made to the efficiency for geometrical add-up of coincident γ-rays. It is seen that our measured value and the predicted value agree within their uncertainty. This result is an independent check on the beam-current integration and γ-ray efficiency calibrations.

3. Targets

In preliminary experiments, the γ-ray backgrounds from 1.3 MeV ^{4}He bombardment of aluminium, zirconium, niobium and gold foils were determined. Previous experience [12]) with ^{3}He-implanted targets indicated these metals were suitable. The foils were polycrystalline with thicknesses of 125 to 250 μm and were annealed and outgassed at 800 °C in high vacuum before bombardment. All targets were found to contain ^{10}B in trace quantities and ^{13}C γ-rays from $^{10}B(^4He, p)^{13}C$ were observed as well as background peaks arising from fast-neutron induced reactions. The gold and niobium foils were found to be the best. However, we have found that niobium can be implanted with more ^{3}He and retains more of the implanted dose during the ^{4}He bombardment than the gold foils.

A set of eight Nb target foils were annealed at 800°C in high vacuum before being implanted with 35 keV ^{3}He at the Chalk River 70 kV isotope separator. Beam current densities were kept below 10 $\mu A/cm^2$. During the implantation to fluences of 7×10^{17} ^{3}He ions/cm^2, the targets were held at room temperature in a vacuum better than 1.3×10^{-5} Pa (10^{-7} Torr) inside a cooled shroud to prevent carbon build-up on the surface of the foils. The targets were implanted uniformly (±4%) over a diameter of 11 mm. Two of the targets were used to establish upper limits of ^{4}He dose, 25 mC ($\sim 5.5 \times 10^{17}$ ^{4}He/cm^2) and current density ~7–9 $\mu A/cm^2$. Under these conditions, less than 20% of the implanted ^{3}He was depleted after ^{4}He bombardment in the apparatus of fig. 1. The remaining six targets were used to determine the cross section for the $^3He(^4He, \gamma)^7Be$ reaction in six separate measurements.

3.1. MEASUREMENT OF THE AREAL CONCENTRATION OF IMPLANTED ^{3}He

All Nb targets with ^{3}He implanted at 35 keV were compared in ^{3}He areal concentration to a similarly implanted Au sample that was used as a secondary standard. The comparison was made with the $^3He(^2H, p)^4He$ reaction at $E_{c.m.} = 300$ keV. The ^{3}He concentration was derived from the number of protons detected at $\theta_{lab} = 150°$ to the beam. The cross section is known absolutely to within 2–3% [refs. [13,14])] and good statistical accuracy can be obtained with small fluences of ^{2}H beam (3×10^{14}/cm^2). Deuterons and ^{4}He particles were stopped by a 0.08 cm thick Al absorber in front of the Si surface-barrier detector.

The yield of protons as a function of the position of a 1 mm diameter beam of ^{2}H was obtained for each target both before and after the ^{4}He bombardment. Fig.

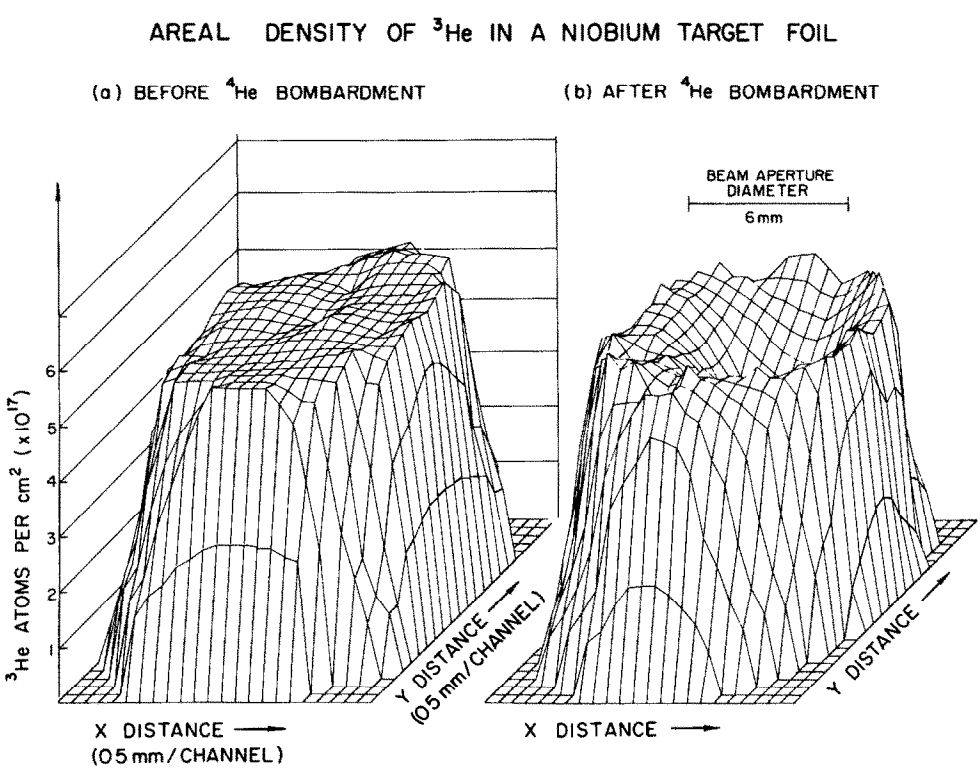

Fig. 3. (a) The areal density of ^{3}He in an implanted niobium target before bombardment with 1.3 MeV ^{4}He. (b) The areal density of ^{3}He in the target after bombardment with 25 mC of 1.3 MeV ^{4}He.

3a shows a plot of the number of ^{3}He atoms/cm^2 before the ^{4}He bombardment (deduced from the proton yield) over the implanted region of one of the targets. It is seen that the uniformity of the implant is good (±4%). Fig. 3b shows the results of a similar assay after the target had been bombarded with 25 mC of 1.3 MeV ^{4}He$^+$ ions. The beam aperture diameter of 6 mm is shown to scale. It is seen that in the central region of the target the concentration of ^{3}He has been reduced.

In fig. 4, the average areal density of a typical ^{3}He target after $T = 6300$ s of bombardment (dose = 25 mC) as a function of the radial distance r from the minimum value of the assay. The assays were sets of measurements of the yield of protons for each position (x, y) on the target. The most depleted point (x_m, y_m) was assumed to be the centre of the beam spot and was chosen as the origin of the radial distance, i.e. $r = \sqrt{(x-x_m)^2+(y-y_m)^2}$. The values at equal distances r were averaged to obtain the areal densities $N_\tau(r, T)$ shown in fig. 4. Before the ^{4}He bombardment, the density was a constant N_0 and r was measured from the geometrical centre of the target. After the bombardment, the ^{3}He-loss profiles $N_0 - N_\tau(r, T)$ were found to be approximately gaussian with a standard deviation

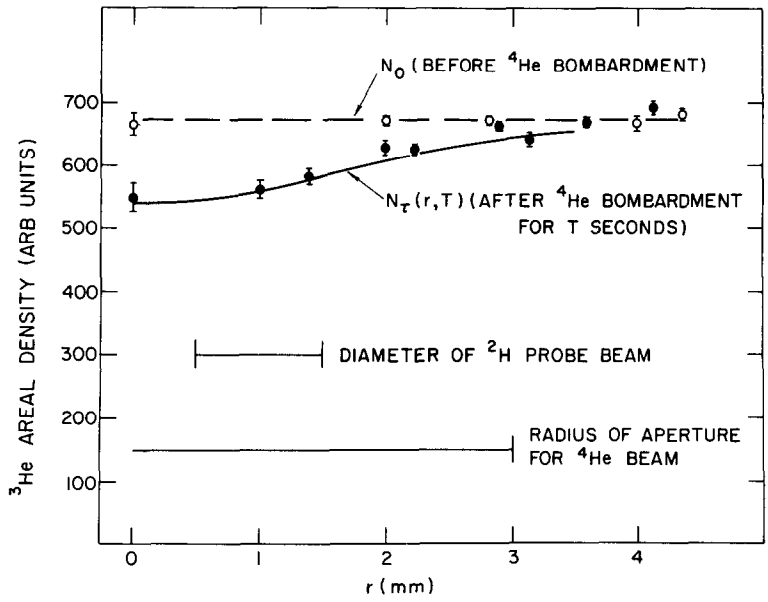

Fig. 4. The ^3He areal density as a function of the radial distance r, from the centre of the beam spot (see text).

of 1.7 mm as shown by the solid curve in fig. 4. The retained fraction of ^3He was determined for a circular area of radius $R = 3.5$ mm.

The results of the ^3He retention measurements are shown in fig. 5 where the retained fraction is plotted versus the ^4He dose. Curve (b) shows the data obtained

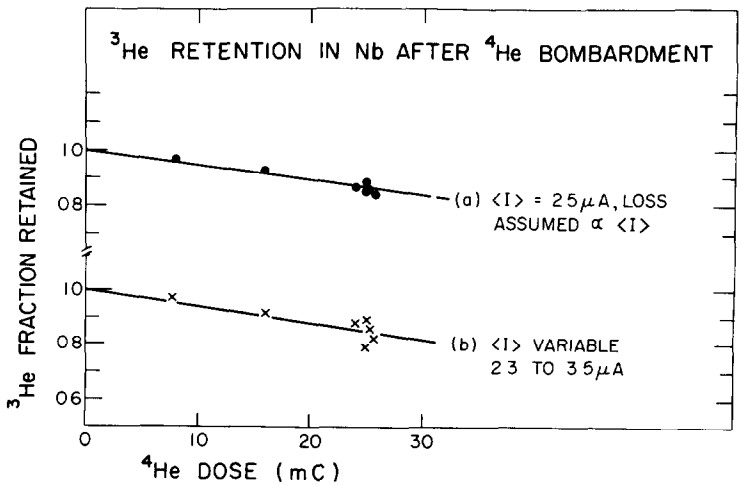

Fig. 5. The fraction of implanted ^3He retained after bombardment with a dose of 8 to 25 mC of 1.3 MeV ^4He. Curve (b) shows raw data taken with average beam currents $\langle I \rangle$ between 2.3 to 3.5 μA for each sample. Curve (a) data have been normalized to $\langle I \rangle = 2.5$ μA, assuming the depletion is also proportional to $\langle I \rangle$, i.e. rate dependent as well as dose dependent.

from the pre- and post-assays by numerically integrating data similar to those illustrated in fig. 3 for one of the targets. For the various runs, the averaged beam currents were not identical but varied between 2.3 and 3.5 μA. If we assume that the depletion is proportional to the beam current as well as the ^{4}He dose, then the data shown in fig. 5a are obtained, normalized to an average current of 2.5 μA. It is seen that the retained fraction falls linearly with dose to the maximum dose used. For larger doses, this linearity is not expected to be maintained. The results of these depletion characteristics are used in the derivation of the ^{3}He(^{4}He, γ)^{7}Be cross section in a later section.

3.2. MEASUREMENT OF THE DEPTH DISTRIBUTION OF THE IMPLANTED ^{3}He TARGETS

The depth profiles have been measured using the ^{3}He(n, p)^{3}H thermal neutron reaction [15]). The results of these measurements are discussed in detail in ref. [16]) and only the results shown in fig. 6 will be discussed here. A flux of $\sim 3 \times 10^7$ neutrons $cm^{-2} \cdot s^{-1}$ from the N4 external thermal neutron facility [17]) at the Chalk River NRU reactor bombarded the ^{3}He-implanted Nb targets. A silicon surface-barrier detector at 90° to the beam measured the energy distributions of the protons and tritons emerging from the targets. The measured energy distribution of the protons was converted to a depth profile for the implanted ^{3}He with stopping powers from Andersen and Ziegler [18]). In fig. 6a the depth profile is shown as measured before the target was bombarded by the 1.3 MeV ^{4}He beam. Fig. 6b shows the depth profile measured for a target after it had been bombarded by ~25 mC of 1.3 MeV ^{4}He. For these data, we recorded only protons originating from the central region of the bombardment area by masking the target with a 4 mm diameter aperture centred on the target. It is seen that the depth distribution of ^{3}He remains unchanged by the ^{4}He bombardment. This is also evident from the observed shape of the direct capture and decay to the ground state, DC → 0 transition, in the ^{3}He(^{4}He, γ)^{7}Be reaction shown in fig. 6c. The γ-ray energy scale has been transformed to a depth scale using stopping power of 1.3 MeV ^{4}He ions [19]). The stopping-power values were verified by energy-loss measurements in Nb foils, whose thicknesses were determined by weighing (~160 μg/cm^2). The primary γ-ray energy (DC → 0) reflects directly the energy distribution of the reacting ^{4}He ions as they traverse the ^{3}He-implanted region. These results will be discussed further in a later section with regard to the determination of the average value of $E_{c.m.}$

3.3. MEASUREMENT OF THE ABSOLUTE TARGET CONCENTRATIONS

As mentioned previously, all ^{3}He-implanted Nb targets were compared in ^{3}He concentration to a similarly implanted Au sample that served as a secondary standard. Several techniques were used to determine the absolute ^{3}He concentration in the Au standard:

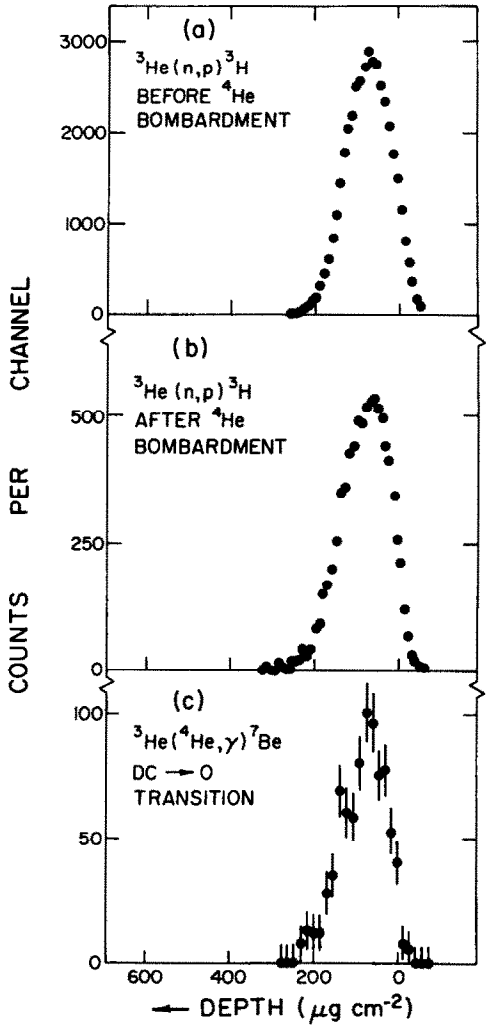

Fig. 6. (a) The depth distribution of 35 keV ^3He in Nb measured before ^4He bombardment with the $^3He(n, p)^3H$ thermal-neutron reaction. The emerging proton energy spectrum has been converted to a depth scale. Background counts have been subtracted. (b) Same as (a) but after ^4He bombardment. Protons emerging from the ^4He bombarded area only were accepted. (c) The observed lineshape of the DC → 0 γ-ray from the $^3He(^4He, \gamma)^7Be$ reaction. Again background has been subtracted and the γ-energy scale has been transformed to a depth scale for comparison with the data of (a) and (b).

(i) Comparison with the elastic scattering of ^2H and ^4He beams from ^{209}Bi, in the same geometry as used for the $^3He(^2H, p)^4He$ reaction. This standard† was a silicon wafer implanted with $(3.60 \pm 0.036) \times 10^{15}$ atoms/cm^2 of ^{209}Bi.

† Series III Bi-implanted Si wafer of precisely known implant dose [20]).

(ii) Comparison with a self-supporting Au target whose thickness was known from ^{4}He transmission energy-loss measurements at 650 keV to be 93.9 $\mu g/cm^2$ based on the Andersen and Ziegler stopping-power tables [19]).

(iii) Comparison with the $^3He(^2H, p)^4He$ reaction yield from the Au standard to the thick-target elastic-scattering spectrum and known deuteron stopping powers [18]) in Au.

(iv) Comparison with the $^{16}O(^2H, p)^{17}O$ reaction yield in the same geometry. The cross section for $^{16}O(^2H, p)^{17}O$ is known absolutely [14]) and precise values for the ^{16}O target atom density can be obtained for Ta_2O_5 layers on Ta formed by anodic oxidation and optical interference techniques [21]).

Using all these techniques, we found that the ^{3}He concentration in the Au secondary standard is 4.61×10^{17} atoms/cm^2, with a standard deviation of 6% that includes the effect of the non-uniformity of the implant. This value is in good agreement with the fluence of $6 \times 10^{17}/cm^2$, measured by current integration during implantation, when allowance for the reflection of the ^{3}He ions is included. The required reflection coefficient of 0.23 is in good agreement with the measurements of Bøttiger *et al.* [22]) who obtained 0.20 for 35 keV ^{3}He in Au.

The initial ^{3}He concentrations (N_0) in the six Nb targets were deduced from the yields of protons from the $^3He(^2H, p)^4He$ reaction for the Nb targets compared with the Au standard. The values are listed in table 1.

4. Measurement of direct-capture γ-rays

4.1. YIELD OF THE $^3He(^4He, \gamma)^7Be$ REACTION

The apparatus shown in fig. 1 was used to measure the direct-capture yield from the $^3He(^4He, \gamma)^7Be$ reaction at a bombarding energy of 1.3 MeV. The spectra from the Ge(Li) detector were accumulated in a 4096-channel pulse-height analyser with a dispersion of 1 keV/channel. Spectra were written onto magnetic tape for later analysis with a PDP-10 computer. The counting rates from the capture reaction and the calibration sources were low, and dead times were always less than 2% as measured by comparison of the number of pulses injected into the pre-amplifier with those counted in the analyser.

A typical run consisted of bombardment of one of the ^{3}He-implanted Nb targets with 25 mC of 1.3 MeV ^{4}He. Fig. 7a shows the spectrum observed; it is actually the sum of two target bombardments. The 4096-channel spectra were compressed by a factor of five for this figure. The running time was recorded for later use in determining the contribution to the spectra from room background. Room background runs were accumulated for periods of about 16 h several times during the series of runs. Fig. 7c is the room background spectrum; the counts have been normalized to the same running time as fig. 7a. The usual background lines from ^{40}K, ^{208}Tl, etc., in building materials are seen.

In fig. 7b, the spectrum observed from the bombardment of a Nb blank target is shown; the counts are normalized to the same accumulated charge as for fig. 7a. Gamma rays of 3854 and 3684 keV are seen from $^{10}B(^{4}He, p)^{13}C$ as well as neutron-induced peaks, e.g. from Ge(n, n'). During some runs, a time-dependent background line at 1294 keV from airborne ^{41}Ar from nearby reactors was observed as in fig. 7b.

In fig. 7a the direct-capture DC → 429 and 429 → 0 keV transitions are clearly seen. The DC → 0 and 429 → 0 keV lines were used to measure the yield and are shown in more detail in fig. 8. Figs. 8a, b and c show the region near the 429 → 0 keV transition for the ^{3}He-implanted Nb target, Nb blank and room background, respectively. The main background under the line is from room background (c) and is slowly decreasing with energy. Figs. 8d, e and f show similar partial spectra in the region near the DC → 0 and DC → 429 keV transitions. Again a major contribution to background under the DC → 0 peak is room background. The DC → 0 peak overlaps the single-escape peak (SE) from the 2614 keV ^{208}Tl line and contributions from the latter were subtracted in the analysis. It was a small contribution of approximately 6–7%.

After two or three ^{3}He targets had been bombarded, the ^{137}Cs and ^{88}Y standardized sources were mounted in the target holder, consecutively, and counted for fixed periods of time to calibrate the detection efficiency and energy.

The areas under the DC → 0 and 429 → 0 peaks were extracted taking into account the tail of the detector response [23]) since these γ-ray lines are much broader than the detector resolution. A shaped background was subtracted which had the form of a running integral matched to the mean background levels below and above the peak. A typical target gave about 180 counts for the DC → 0 transition and 290 counts in the 429 → 0 keV transition. The cross-section values deduced from each target are listed in table 1. Targets 1 and 2 were not used to determine cross-section values, although they were used to determine additional branching-ratio data.

4.2. MEASUREMENT OF THE c.m. ENERGY

The c.m. energy of a direct capture reaction can be determined by measuring the DC → 0 transition energy. The transition energy is $E_\gamma^0 = Q + E_{c.m.} - E_R$ where, in the present case, $Q = 1586.3 \pm 0.5$ keV [ref. [6])], $E_{c.m.} = (m_3/m_7)E_\alpha$, m_3 is the mass of ^{3}He, m_7 is the sum of the masses of ^{3}He and ^{4}He, E_R is the recoil energy given to ^{7}Be by the γ-emission, and E_α is the bombarding energy. The centroid of the energy of the DC → 0 γ-ray measured at $\theta = 0°$ is, to first order in the average ^{7}Be recoil velocity, $\bar{\beta}c$:

$$\overline{E_\gamma(0°)} = \langle E_\gamma^0(1 + \bar{\beta}Q_l)\rangle ,$$

where Q_l is the value of cos θ averaged over the finite solid angle subtended by the Ge(Li) detector. With the energy calibration of the ^{208}Tl 2614.5 keV and ^{40}K 1461 keV γ-ray lines observed concurrently with the reaction γ-rays, the measured energy $\overline{E_\gamma(0°)}$ was found to be 2136.7 ± 1.9 keV and gives $E_{c.m.} = 525 \pm 3$ keV.

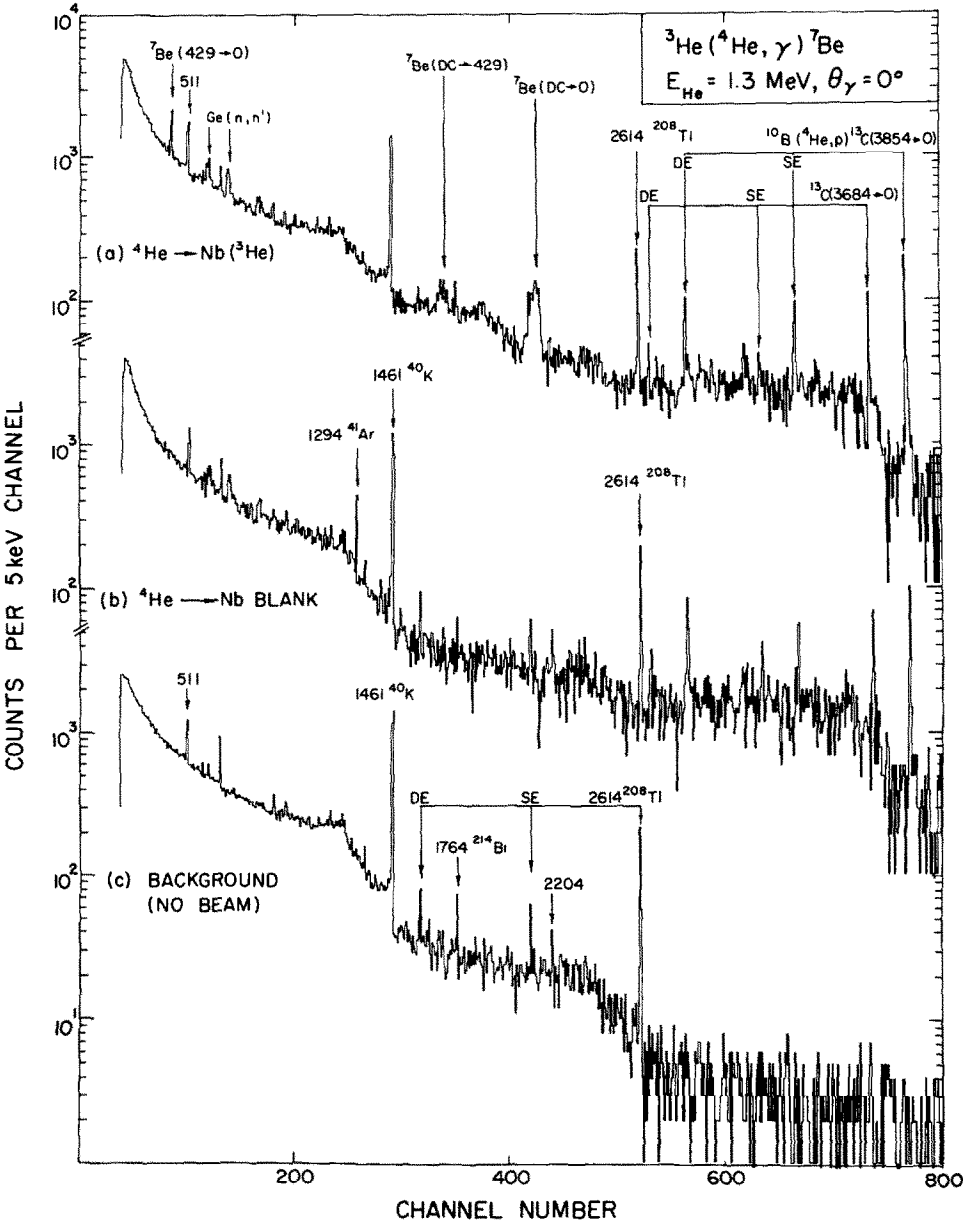

Fig. 7. (a) The γ-ray spectrum observed at $\theta_\gamma = 0°$ from the 1.3 MeV ^4He bombardment of the ^3He-implanted Nb target. The $^3He(^4He, \gamma)^7Be$ DC $\rightarrow$ 429 and 429 $\rightarrow$ 0 keV transitions are evident. Gamma rays from reactions with ^{10}B impurities and peaks from (n, n'γ) reactions are seen. The 4096-channel spectrum has been compressed to give 5 keV/channel dispersion. (b) The γ-rays from a similar bombardment of a Nb blank target for the same charge as in (a). The dispersion is 5 keV/channel. (c) The γ-rays from room background (no beam) normalized to the same counting time as (a). The ^{40}K and ^{208}Tl lines, etc., are from building materials.

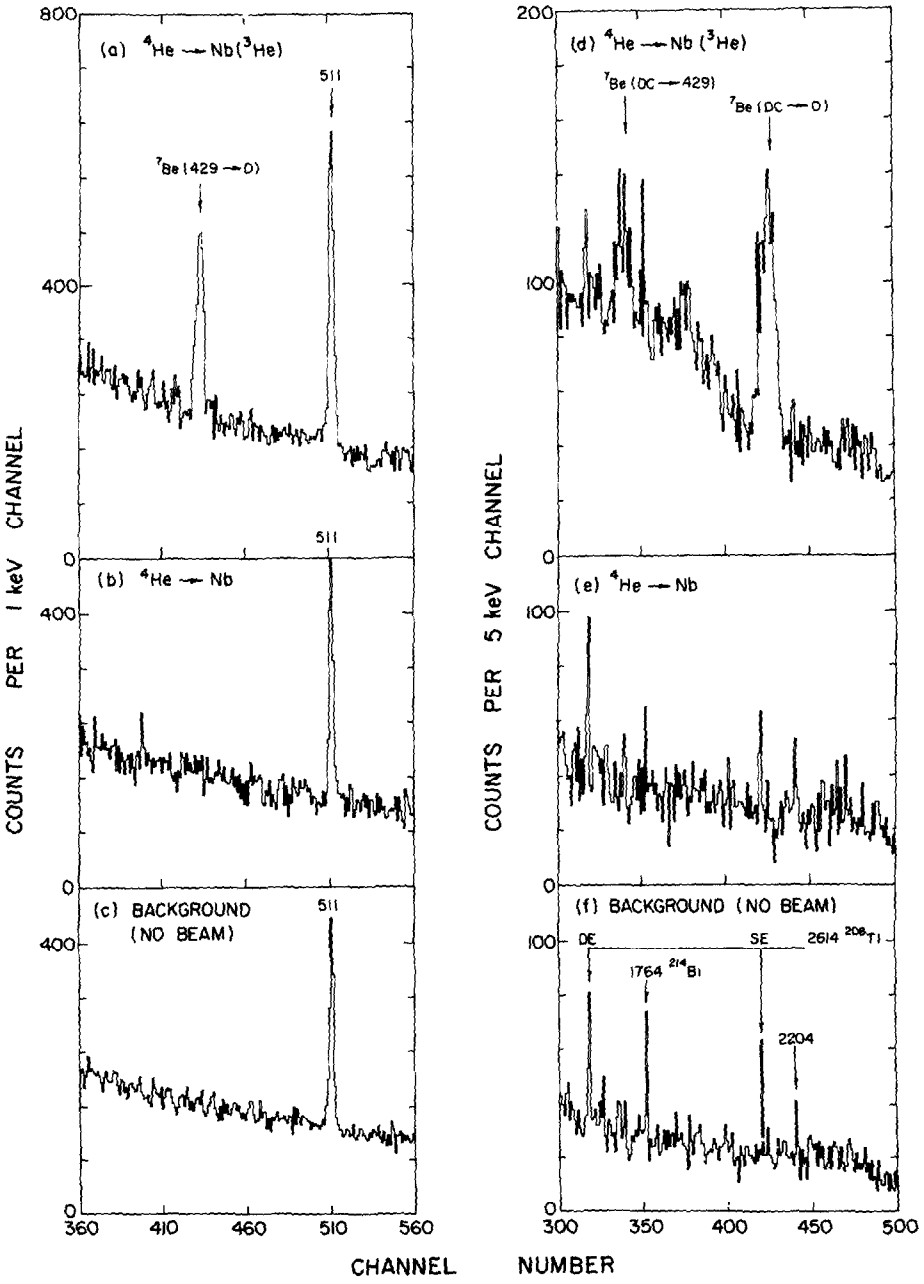

Fig. 8. Partial γ-ray spectra in the region of the 429 → 0 keV transition: (a) for the ^3He-implanted target, (b) for the Nb blank, and (c) for room background. (d) (e) and (f) are partial γ-ray spectra in the region of the DC → 0 transition for the conditions corresponding to (a), (b) and (c).

5. Analysis of the data

The cross section $\sigma(E_{c.m.})$ and the yield of γ-ray counts/s, dy, from reactions in a layer of thickness dz located at a depth z inside the Nb foil are related by

$$dy = n_\tau(z) I_\alpha \sigma(E_{c.m.}) \eta(E_\gamma)\, dz,$$

where $n_\tau(z)$ is the number of ^{3}He target atoms/cm^3 at depth z, I_α is the number of ^{4}He particles per second, and $\eta(E_\gamma)$ is the γ-ray detector efficiency at the energy E_γ. The c.m. energy is

$$E_{c.m.}(z) = 0.4297[E_\alpha - z\varepsilon_\alpha],$$

where E_α is the ^{4}He bombarding energy and ε_α is the stopping power of ^{4}He by Nb. The γ-ray energy is

$$E_\gamma = (E_{c.m.}(z) + Q - E_R)(1 + \beta(z) Q_1).$$

The yield, y, integrated over the distribution $n_\tau(z)$ is

$$y = \eta_0 I_\alpha N_\tau \bar{\sigma},$$

where $\eta(E_\gamma) = \eta_0 \overline{E_\gamma(0°)}/E_\gamma$, η_0 is the efficiency at energy $\overline{E_\gamma(0°)}$, $N_\tau = \int_0^\infty n_\tau(z)\, dz$, and

$$\bar{\sigma} = \frac{S_{34}(\overline{E_{c.m.}})}{N_\tau \eta_0} \int_0^\infty \frac{n_\tau(z)\eta(E_\gamma)\, dz}{E_{c.m.} \exp(164.12/\sqrt{E_{c.m.}})}.$$

The γ-ray full-energy peak detection efficiency depends on E_γ (and thus on z) and has been kept inside the integral. The cross-section factor $S_{34}(E_{c.m.})$ has been assumed to be equal to $S_{34}(\overline{E_{c.m.}})$, a constant over the integration. The centroid of the DC → 0 γ-ray distribution can be calculated from

$$\overline{E_\gamma(0°)} = \frac{S_{34}(\overline{E_{c.m.}})}{N_\tau \bar{\sigma} \eta_0} \int_0^\infty \frac{E_\gamma n_\tau(z)\eta(E_\gamma)\, dz}{E_{c.m.} \exp(164.12/\sqrt{E_{c.m.}})}.$$

The integrals have been evaluated numerically with the experimental depth distributions shown in figs. 6a and b, the stopping power of ^{4}He (ε_α = 0.742 keV/μg/cm^2) and the beam energy 1286 ± 2.6 keV measured with a time-of-flight spectrometer as described in ref. [24]). This calculation gives $\overline{E_\gamma(0°)} = 2137.6$ keV corresponding to $E_{c.m.} = 526 \pm 4$ keV in agreement with the directly measured value $E_{c.m.} = 525 \pm 3$ keV. Since the latter is independent of the energy-loss determination and the accelerator calibration, the value of E_α used to determine $S_{34}(E_{c.m.})$ was adjusted until the calculated value $\overline{E_\gamma(0°)}$ agreed with the experimental value.

Since the number of target atoms depletes during the bombardment, the total yield during the run time T [s] is

$$Y = \int_0^T y\, dt = \bar{\sigma}\eta_0 \int_0^T \int_0^R N_\tau(r, t) j(r, t) 2\pi r\, dr\, dt,$$

where the beam has been assumed to be cylindrically symmetric with radius R and flux $j(r, t)$. In addition to Y, we have also measured the integrated number of incident ^{4}He ions,

$$N_\alpha = \int_0^T \int_0^R j(r, t) 2\pi r \, dr \, dt,$$

the number of ^{3}He atom/cm^2 remaining after T seconds of bombardment, $N_\tau(r, T)$, and the initial target concentration $N_\tau(r, 0)$, which is equal to a constant N_0 independent of r from the pre-assay of the target.

As discussed previously and shown in fig. 5, the fraction of ^{3}He atoms remaining after bombardment depends linearly on the ^{4}He fluence. If we assume that the beam current is constant with time, then

$$N_\tau(r, t) = N_0(1 - mj(r)t),$$

where m is determined experimentally; i.e. the target density depletes linearly with time and the depletion follows the beam current density $j(r)$. Using this expression in the equation for Y and taking the beam density to be gaussian, $j(r) = j_0 e^{-r^2/2\Sigma^2}$, we obtain

$$\begin{aligned} Y &= \bar{\sigma}\eta_0 N_\alpha N_0 \{1 - \tfrac{1}{4} m T j_0 (1 + e^{-R^2/2\Sigma^2})\} \\ &= \bar{\sigma}\eta_0 N_\alpha N_0 f. \end{aligned}$$

The correction factor f can be written as

$$f = \left[1 - \frac{N_0 - N_\tau(0, T)}{4N_0}(1 + e^{-R^2/2\Sigma^2})\right],$$

where $N_\tau(0, T)$ and N_0 are directly measured from the assays of the targets. It can also be expressed in terms of the retained fraction $F_\tau(T)$ of ^{3}He where

$$F_\tau(T) = \frac{\int_0^R N_\tau(r, T) 2\pi r \, dr}{N_0 \pi R^2},$$

$$f = \left[1 - \tfrac{1}{4}(1 - F_\tau(T)) \frac{R^2}{2\Sigma^2} \frac{(1 + e^{-R^2/2\Sigma^2})}{(1 - e^{-R^2/2\Sigma^2})}\right].$$

Experimentally it was found (see subsect. 3.1) that the loss profiles $(N_0 - N_\tau(r, T))$ and hence the beam profile $j(r)$ was approximately gaussian with a standard deviation $\Sigma = 1.7$ mm. The retained fractions were determined for a radius of $R = 3.5$ mm. On the average the two methods of determining f gave values that agreed within 2%. The values of f derived for each target are listed in table 1 and show the average effective target depletion was less than 10%; an uncertainty of ±3% was assigned to f.

TABLE 1

Summary [a]) of results for $E_{c.m.} = 525$ keV

Target	N_α ($\times 10^{17}$)	N_0 ($\times 10^{17}$/cm^2)	f	$\bar{\sigma}$(DC→429) (nb)	$\bar{\sigma}$(DC→0) (nb)
3	1.133	6.32±0.51 (0.34) [b])	0.92	171±(24) [c])	395±(48) [c])
4	1.513	5.79±0.49 (0.35)	0.88	124±(22)	316±(44)
5	1.561	5.78±0.46 (0.30)	0.88	153±(22)	337±(40)
6	1.382	5.90±0.47 (0.31)	0.91	134±(22)	337±(43)
7	1.498	5.86±0.47 (0.31)	0.92	144±(19)	414±(47)
8	0.999	5.90±0.47 (0.31)	0.95	123±(22)	389±(54)
				average [d]) 141±13(9)	360±32(19)
		$\bar{\sigma}$(DC→429)/$\bar{\sigma}$(DC→0) = ratio, $R = 0.39 \pm 0.03$			
1 and 2				ratio, $R = 0.42 \pm 0.03$	
				average, $R = 0.41 \pm 0.02$	

[a]) N_α, N_0, f and $\bar{\sigma}$ are defined in the text.

[b]) The uncertainties in the brackets are statistical; total uncertainty includes 6% for absolute measurement.

[c]) The uncertainties in brackets include statistical errors in N_0, Y and 3% in f.

[d]) Weighted average; the chi-squared per degree of freedom is $\chi^2_N = 0.65$ and 0.75 for $\bar{\sigma}$(DC→429) and $\bar{\sigma}$(DC→0), respectively.

The efficiencies of the Ge(Li) detector at the energies of the 429 keV and DC→0 transitions were obtained by extrapolation from the absolutely measured values at 662, 898 and 1836 keV from the ^{137}Cs and ^{88}Y sources, respectively. The effective efficiency for the 429→0 transition was corrected for add-up of the DC→429 transition. Both yields were corrected for the aberration effect on the solid angle of the detector

$$\frac{d\Omega}{d\Omega_{lab}} = \frac{1-\beta^2}{(1-\beta\cos\theta)^2} \simeq 1 + 2\beta Q_1 ,$$

where $2\beta Q_1 = 0.025$ for the DC→0 transition and 0.014 for the 429→0 transition. The correction is smaller for the 429→0 transition because the level lives longer and the average recoil velocity of the emitting ^{7}Be nuclei is smaller.

The 0° yield of the DC→0 transition was corrected for angular distribution anisotropy by using the calculated angular-distribution coefficients of Tombrello and Parker [3]). This correction increases the value of the observed yield by 2.2%. The 429 keV γ-ray is isotropic and its yield was only corrected for the aberration effect.

Table 1 summarizes the $\bar{\sigma}$(DC→429), $\bar{\sigma}$(DC→0) and $R = \bar{\sigma}$(DC→429)/ $\bar{\sigma}$(DC→0) measurements for $\overline{E_{c.m.}} = 525 \pm 3$ keV. The total cross section is

$$\sigma(\overline{E_{c.m}} = 525) = 501 \pm 41(21)\text{nb}, \qquad R = 0.41 \pm 0.02 .$$

The uncertainty of 21 nb is from the counting statistics. Additional uncertainties of 6% for the absolute determination of N_0, 3.4% for absolute determination of η_0, and 1% for current integration have been added in quadrature to obtain the total uncertainty of 41 nb. The equation relating $\bar{\sigma}$ and $S_{34}(\overline{E_{c.m.}})$ yields

$$S_{34}(\overline{E_{c.m.}} = 525) = 341 \pm 29 \text{ eV} \cdot \text{b},$$

where the uncertainty from $\overline{E_{c.m.}}$ has been included. This leads to a value of $S_{34}(0) = 470 \pm 39$ eV · b if the extrapolation due to Tombrello and Parker [3]) is used.

6. Discussion

The present value of $S_{34}(0)$ was obtained from a new experimental method in which the density of the target atoms was determined before and after the measurement of the γ-ray yield. The cross section was deduced from measured values of the yield, the target atom density, the flux of projectiles and the detection efficiency. The extrapolation of $S_{34}(525)$ to $S_{34}(0)$ was made according to the theoretical calculation of Tombrello and Parker [3]). The same calculation was used to take into account the angular distribution of the γ-rays.

The value of $S_{34}(0)$ from the present experiment is compared with the values obtained previously in fig. 9, where the weight of the measured value is plotted versus the measured value [25]). The reference value is the weighted average of the prompt capture γ-ray yield measurements 0.47 ± 0.05 [ref. [4])], 0.58 ± 0.07 [ref. [5])], 0.52 ± 0.03 [ref. [7])] and 0.47 ± 0.04 keV · b, the present value. The contours are at plus and minus two standard deviations from the reference value $S_{34}(0) = 0.50 \pm 0.02$ keV · b.

All direct-capture prompt γ-ray measurements are in agreement with this reference value except the value 0.30 ± 0.03 keV · b quoted by Kräwinkel *et al.* [6]). However, the value $S_{34}(0) = 0.38 \pm 0.06$ keV · b deduced from the absolute cross-section measurement of Kräwinkel *et al.* ($\sigma(195.2) = 13.6 \pm 2.2$ nb) is in agreement with the reference value. (Their quoted value was a weighted average of the absolute value and many values determined relative to other reaction cross sections.)

It is evident from fig. 9 that the average value of $S_{34}(0) = 0.57 \pm 0.02$ keV · b from the ^7Be activation measurements, 0.55 ± 0.05 [ref. [7])], 0.63 ± 0.04 [ref. [8])] and 0.56 ± 0.03 [ref. [9])] keV · b, is larger than the reference value from the prompt capture γ-ray measurements. In general, the activation measurements have been extrapolated from higher values of $E_{c.m.}$ than those for the prompt γ-ray measurements, and perhaps the systematic shift ($\sim$14%) may result in part from a deviation of the theoretical shape of $S(E_{c.m.})$ from the real shape. However, prompt γ-ray measurements over a broad range of $E_{c.m.}$ [refs. [4,6,7])] have not uncovered large systematic deviations from the theoretical shape of $S(E_{c.m.})$.

In conclusion we find that the measurements of $S_{34}(0)$ by the direct determination of capture γ-yields are consistent with each other and lead to a weighted average

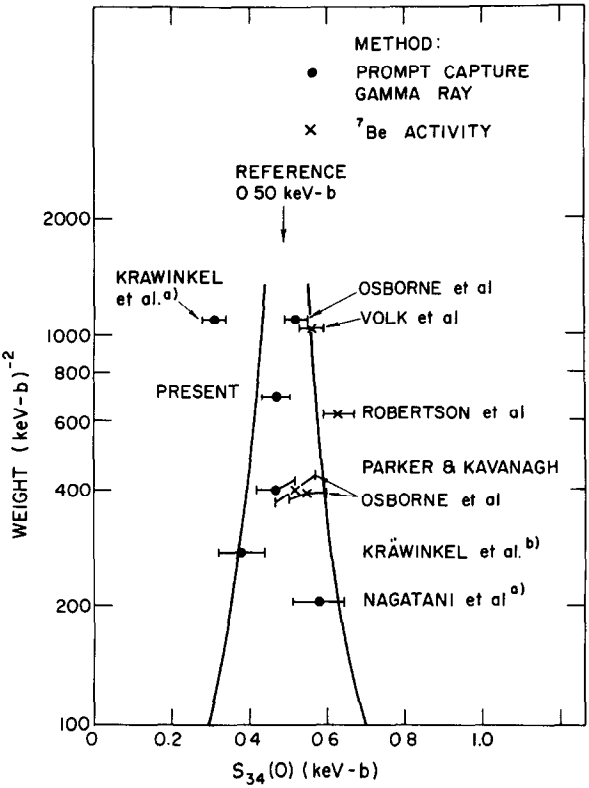

a) The $S_{34}(E_{c.m.})$ values of Nagatani *et al.* [5]) and Kräwinkel *et al.* [6]) have been extrapolated in the manner outlined by Robertson *et al.* [8]) to obtain $S_{34}(0)$.

[b]) The absolute determination quoted by Kräwinkel *et al.* (see text).

Fig. 9. Comparison of the present value of $S_{34}(0)$ with previous measurements. The weight of the measurement is plotted versus the value obtained [25]). The lines are $\pm 2\sigma$ contours around the reference value.

of $S_{34}(0) = 0.50 \pm 0.02$ keV · b. Determinations by measurement of the induced ^{7}Be activity are also consistent with each other, but lead to a weighted average of $S_{34}(0) = 0.57 \pm 0.02$ keV · b, a value three-and-a-half standard deviations different. Since the capture γ-ray yield method results in cross-section factors requiring the smallest extrapolation to low values of $E_{c.m.}$, we recommend a value of 0.50 keV · b for the zero-energy cross-section factor. Robertson *et al.* [8]) have discussed the issue of extrapolating measured values to obtain $S_{34}(0)$ and suggest an uncertainty of 10% be assigned to $S_{34}(0)$ from this source. Thus an estimate of the one standard deviation uncertainty on the experimental value 0.50 keV · b is ±0.05 keV · b. Our recommended value is slightly below the value 0.52 keV · b chosen by Bahcall *et al.* [1]) to calculate the expected solar neutrino event rate. However, the expected rate is lowered by only 5%.

We wish to acknowledge the valuable technical assistance provided by N.C. Bray, J.L. Gallant, D. Phillips, H.H. Plattner, G.A. Sims, L.V. Smith, and O.M. Westcott. The calibrated γ-ray sources were prepared by R.H. Martin.

References

1) J.N. Bahcall, W.F. Huebner, S.H. Lubow, P.D. Parker, and R.K. Ulrich, Rev. Mod. Phys. **54** (1982) 767
2) R. Davis, Jr., Proc. Conf. on science underground, Los Alamos, 1982, vol. 96 (AIP, 1983)
3) T.A. Tombrello and P.D. Parker, Phys. Rev. **131** (1963) 2582
4) P.D. Parker and R.W. Kavanagh, Phys. Rev. **131** (1963) 2578
5) K. Nagatani, M.R. Dwarakanath and D. Ashery, Nucl. Phys. **A128** (1969) 325
6) H. Kräwinkel, H.W. Becker, L. Buchmann, J. Görres, K.U. Kettner, W.E. Kieser, R. Santo, P. Schmalbrock, H.P. Trautvetter, A. Vlieks, C. Rolfs, J.W. Hammer, R.E. Azuma and W.S. Rodney, Z. Phys. **A304** (1982) 307
7) J.L. Osborne, C.A. Barnes, R.W. Kavanagh, R.M. Kremer, G.J. Mathews, J.L. Zyskind, P.D. Parker and A.J. Howard, Phys. Rev. Lett. **48** (1982) 1664; Nucl. Phys. **A419** (1984) 115
8) R.G.H. Robertson, P. Dyer, T.J. Bowles, R.E. Brown, N. Jarmie, C.J. Maggiore and S.M. Austin, Phys. Rev. **C27** (1983) 11
9) H. Volk, H. Kräwinkel, R. Santo, and L. Walleck, Z. Phys. **A310** (1983) 91
10) B.M. Paine and D.G. Sargood, Nucl. Phys. **A331** (1979) 389
11) A. Anttila, J. Keinonen, M. Hautala and I. Forsblom, Nucl. Instr. Meth. **147** (1977) 501
12) T.K. Alexander, G.C. Ball, W.G. Davies and I.V. Mitchell, J. Nucl. Mat. **96** (1981) 51
13) W. Möller and F. Besenbacher, Nucl. Instr. Meth. **168** (1980) 111
14) J.A. Davies and P.R. Norton, Nucl. Instr. Meth. **168** (1980) 611
15) J.P. Biersack, D. Fink, R. Henkelmann and K. Müller, Nucl. Instr. Meth. **149** (1978) 93
16) H. Geissel, W.N. Lennard, T.K. Alexander, G.C. Ball, J.S. Forster, M.A. Lone, L. Milani, D. Phillips and H.H. Plattner, Nucl. Instr. Meth. **B2** (1984) 770
17) M.A. Lone, D.C. Santry and W.M. Inglis, Nucl. Instr. Meth. **174** (1980) 521
18) H.H. Andersen and J.F. Ziegler, Hydrogen: stopping powers and ranges in all elements (Pergamon, NY, 1977)
19) J.R. Ziegler, Helium: stopping powers and ranges in all elements (Pergamon, NY 1977)
20) C. Cohen, J.A. Davies, A.V. Drigo and T.E. Jackman, Nucl. Instr. Meth. **218** (1983) 147
21) D. Phillips and J.P.S. Pringle, Nucl. Instr. Meth. **135** (1976) 389
22) J. Bøttiger and N. Rud, Inst. of Phys. Conf. Series **28** (1976) 224
23) J.M. Szöghy, J.S. Forster and G.C. Ball, Nucl. Phys. **A201** (1973) 433
24) W.N. Lennard, D. Phillips and R. Hill, IEEE Trans. on Nucl. Sci. **NS-30** (1983) 1532
25) T.K. Alexander and J.S. Forster, Advances in nuclear physics, vol. 10, ed. M. Baranger and E. Vogt (Plenum, NY 1978) pp. 197–331